EPJ AP
Applied Physics
EPJ.org
your physics journal

Eur. Phys. J. Appl. Phys. (2012) 59: 10301 DOI: 10.1051/epjap/2012120082

Chemical bond approach to optical properties of some flash evaporated $Se_{100-x}Sb_x$ chalcogenide alloys

C.M. Muiva, T.S. Sathiaraj, and J.M. Mwabora

edp sciences

The title "The European Physical Journal" is a joint property of EDP Sciences, Società Italiana di Fisica (SIF) and Springer

Eur. Phys. J. Appl. Phys. (2012) 59: 10301
DOI: 10.1051/epjap/2012120082

THE EUROPEAN PHYSICAL JOURNAL
APPLIED PHYSICS

Regular Article

Chemical bond approach to optical properties of some flash evaporated $Se_{100-X}Sb_X$ chalcogenide alloys

C.M. Muiva[1,3], T.S. Sathiaraj[1,3,a], and J.M. Mwabora[2,3]

[1] Department of Physics, University of Botswana, P/Bag UB-0022 Gaborone, Botswana
[2] Department of Physics, University of Nairobi, PO Box 30197-00100 Nairobi, Kenya
[3] African Materials Science and Engineering Network (AMSEN), a Carnegie IAS-RISE Network, UB-Node, P/Bag UB-0022, Gaborone, Botswana

Received: 2 March 2012 / Received in final form: 5 June 2012 / Accepted: 6 June 2012
Published online: 11 July 21012 –

Abstract. Amorphous thin films of $Se_{100-X}Sb_X$ (X = 1, 5, 10, 15 and 20) were synthesized by flash evaporation of the premelt quenched bulk samples. The optical properties were investigated from spectrophotometric measurements in the UV-VIS-NIR spectral region using Swanepoel's standard envelope method and related techniques. The optical band gap energy (E_g^{opt}) was evaluated from the Wemple-Didomenico (WDD) single oscillator model and Tauc's extrapolation method in the region where the absorption coefficient, $\alpha \geq 10^4$ cm^{-1}. The observed values of E_g^{opt} and oscillator energy E_o were found to decrease monotonously with increasing Sb additive. The complex dielectric constant (ε), Urbach energy (E_u), optical conductivity (σ), plasma frequency (ω_p) and lattice dielectric constant (ε_L) were deduced for each alloy composition. The complex refractive index (n) fitted well to Sellmeier function which can allow extrapolation of n outside the measured spectral range. The observed changes in optical parameters with Sb content were explained on the basis of increased defect states and changes in cohesive energy indicators (average heat of atomization (H_s), mean coordination number $\langle Z \rangle$ and average single bond energy ($H_s/\langle Z \rangle$).

1 Introduction

Semiconducting chalcogenide alloys have a wide range of technological applications including fiber optics, infrared optics, optical data storage, X-ray imaging, TV vidicon pick-up tubes, optical power switches, amplifiers and xerography. These applications are based on their opto-electronic properties which are easily modifiable through varying alloy composition, preparative conditions or post-deposition treatment. Absence of long range order as well as intrinsic defects in the amorphous microstructure generates localized states in the mobility gap with consequent effects on the optical and electrical properties [1]. In spite of this lack of long range order inherent in their crystalline counterparts, there is a large degree of short range spatial order in atomic structure arising from quest of each atom to fulfill its valence requirements. Recently, several reports on the Se-Sb binary systems have surfaced [2–5] owing to the large recipe for technological applications. The underlying rationale is the technological advantage of their opto-electronic, dielectric and thermal properties. On top of these properties, changes in reported opto-electronic properties with reversible transformation from amorphous to the crystalline state have elicited attention toward applications in phase change memory and threshold switching [6,7] devices.

Alloying of amorphous selenium (a-Se) with Sb has been reported to significantly improve mechanical robustness, raise crystallization temperature, enhance conductivity and reduce aging effects as compared to pure a-Se [3,8]. Selenium-based alloys with high Sb content are reported to have ultrafast crystallization rates (as low as 8 ps laser pulses) [9]. Recently, Tintu et al. [10] have described optical limiting absorption in Sb-based glasses. Othman [11] has investigated photodarkening effects on $Se_{90}Sb_{10}$ due to high UV doses. Mikla et al. [6] observed enhanced xerographic photosensitivity in Sb_XSe_{100-X} alloys at longer wavelengths ($\lambda > 670$ nm) than for pure Se, while Kang et al. [7] have described structural transformation and related kinetics of Sb_XSe_{100-X} with high Sb alloying for feasibility studies geared toward application in phase change non-volatile memories. Srivastava et al. [2] and Fouad et al. [5] have adopted a theoretical approach to study optical band gap in Se-Sb glasses.

An adequate pool of knowledge of the optical properties of Se-Sb system is crucial toward full realization of the technological potential of this binary system. In the present work, the effects of Sb addition on the

[a] e-mail: sathiara@mopipi.ub.bw

optical properties in some flash evaporated $Se_{100-X}Sb_X$ ($X = 1$, 5, 10, 15 and 20) chalcogenide alloys are reported. The observed modification of optical parameters arising from increased Sb additive has been correlated to the consequent change in bond energy parameters.

2 Experimental details

Bulk glassy alloys of $Se_{100-X}Sb_X$ ($X = 1$, 5, 10, 15 and 20) were prepared from high purity (99.999%) elemental components by the conventional melt quenching technique whose specific details are described elsewhere [12]. Se-Sb thin films were then synthesized by flash evaporation of the powdered bulk samples in a high vacuum Edwards Auto 306 coating chamber evacuated to a base pressure of 10^{-5} Torr. The samples were weighed into the flash evaporation attachment and delivered continuously into preheated tantalum boats placed between two electrodes in the vacuum chamber. The samples were then evaporated through resistance heating onto precleaned microscopic glass slides held above the boats. It was ensured that there was no intentional heating of the substrates and that the temperature in the vicinity of the samples was below 35 °C to prevent phase transformation.

The formation of an amorphous phase was confirmed through X-ray diffraction (XRD) studies. The X-ray sources featured a copper anode with characteristic Kα radiation of wavelength 1.50654 Å. The elemental composition of the films was confirmed from scanning electron microscopy (SEM) using a Philips XL 30 SEM microscope fitted with an EDS system for compositional analysis. The normal transmission and reflectance data were measured using a Shimadzu SolidSpec-3700 DUV, UV-VIS-NIR spectrophotometer in the spectral range 300–2500 nm. The film thickness was obtained from the envelope method and confirmed by direct measurement from a KLA Tencor P-15 stylus profiler.

3 Results and discussion

Figure 1 shows XRD patterns of the the $Se_{100-X}Sb_X$ system compared against that of the blank glass substrates used. The hump in the XRD patterns between 2θ values of 20–35 was attributed to the glass substrate hosting the films. The absence of distinct diffraction peaks indicates formation of an amorphous phase in these glasses. This was correlated by SEM pictographs (not shown here) which showed a smooth surface devoid of microsized crystallites.

The spectral dependence of transmittance (T) for the pristine $Se_{100-X}Sb_X$ thin films in the spectral range 300–2500 nm is shown in Figure 2. A distinct absorption edge in the wavelength range 580–750 nm was observed which is an indication of good optical filtering behavior. A red shift in the absorption edge with increasing Sb content was observed. The observed interference fridges were assigned to difference in refractive index (n) between the glass substrate and film ($d \approx 0.981\,\mu$m).

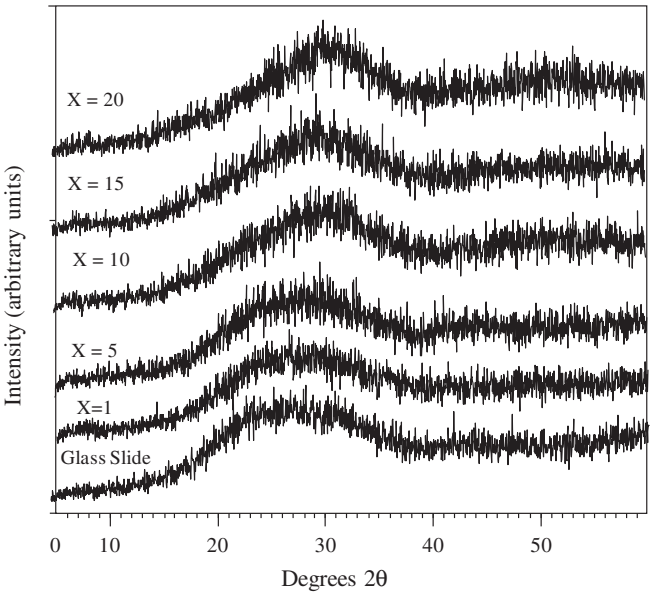

Fig. 1. XRD diffractographs of the $Se_{100-X}Sb_X$ thin film alloys compared against a blank glass slide used as substrates.

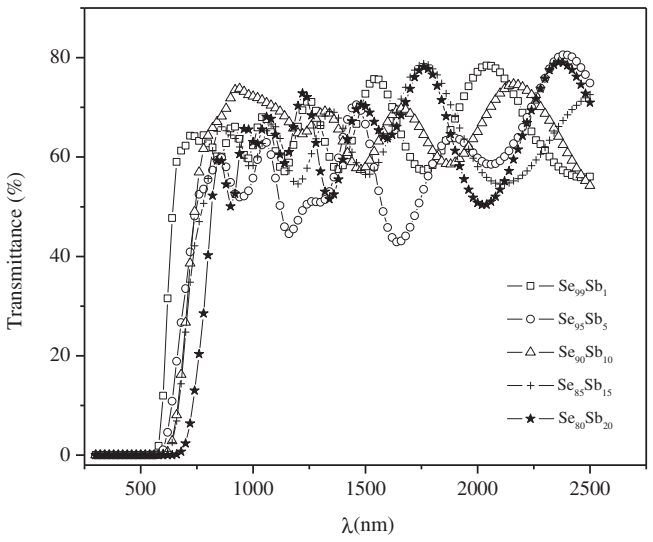

Fig. 2. Transmission spectra of $Se_{100-X}Sb_X$ thin film alloys.

The values of absorption coefficient α which are correlated to the extent of loss of incident intensity as a beam is propagated through the dimensions of a material were calculated from transmittance (T), reflectance (R) spectra and film thickness (d) using the relation [13]:

$$\alpha = (1/d)\ln\left[\left\{-(1-R)^2 + \sqrt{(1-R)^4 + 4(TR)^2}\right\}/2T\right]. \quad (1)$$

The estimated optical band gap (E_g^{opt}) was then obtained from the spectrophotometric α data in the region where $\alpha \geq 10^4$ cm^{-1} using the relation [14,15]:

$$\alpha h\nu = B(h\nu - E_g^{opt})^n, \quad (2)$$

where B is the band tailing parameter which depends on electronic transition probability and can be obtained

Table 1. WDD dispersion parameters (E_o and E_d), Urbach energy (E_u), lattice dielectric function (ε_L), static refractive index $n(0)$, high frequency dielectric constant $(n(0)^2)$, E_g^{opt} (Tauc), $E_g'^{opt}$ (WDD) and $E_g''^{opt}$ (Eq. (10)) optical band gap energies, band tailing parameter (B), and plasma frequency (ω_p) of $Se_{100-X}Sb_X$ thin films.

Sb (at.%)	E_d (eV)	E_o (eV)	E_u (eV)	ε_L	$n(0)$	$n(0)^2$	σ opt $\times 10^{11}$ (Hz)	E_g^{opt} Tauc (eV)	$E_g'^{opt}$ (WDD) (eV)	$E_g''^{opt}$ (Eq. (10)) (eV)	B (eV cm)$^{-1/2}$	$\omega_p \times 10^{13}$ S^{-1}
1.0	21.40	3.89	0.25	6.94	2.55	6.50	1.01	1.89	1.95	1.88	816	10.89
5.0	23.04	3.62	0.48	7.91	2.72	7.37	2.06	1.81	1.81	1.79	619	8.57
10.0	21.97	3.25	0.38	8.27	2.79	7.76	1.52	1.59	1.63	1.59	576	8.82
15.0	22.59	3.16	0.55	8.47	2.85	8.14	3.50	1.46	1.58	1.47	405	8.36
20.0	20.98	2.98	0.52	8.72	2.84	8.04	7.88	1.41	1.49	1.45	691	7.98

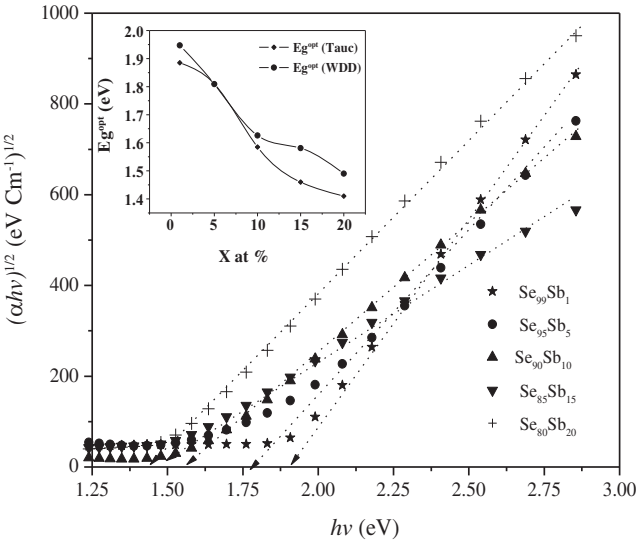

Fig. 3. Variation of $(\alpha h\nu)^{1/2}$ with incident photon energy ($h\nu$) for $Se_{100-X}Sb_X$ thin films. Inset: WDD and Tauc optical band gap energies as a function of Sb content. Dotted lines are the linear extrapolations for $\alpha \to 0$.

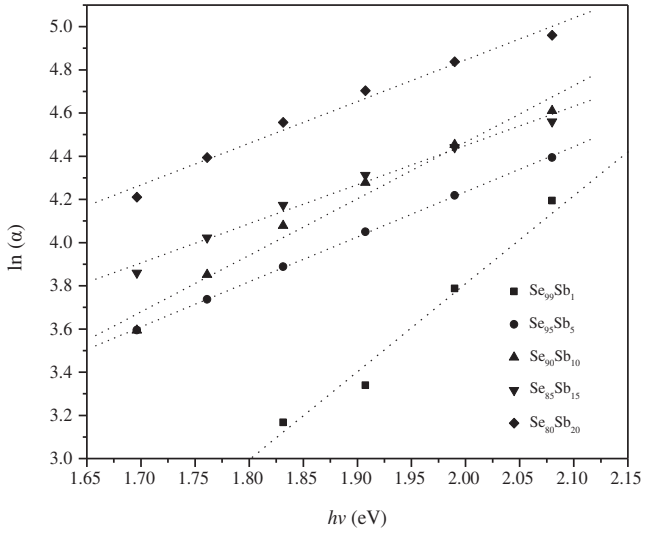

Fig. 4. Dependence of $\ln(\alpha)$ with photon energy ($h\nu$) for $Se_{100-X}Sb_X$ thin films. Dotted lines are linear fitting of the plotted points, $R \approx 0.993$.

directly from the slope of Tauc's plot (Fig. 3). The superscript, n in equation (2) is associated with the nature of electronic excitations across the energy gap. The observed absorption data fitted well to $n = 2$ corresponding to indirect allowed transition which is also the value usually reported for this type of glassy samples [2,5]. Plot of $(\alpha h\nu)^{1/2}$ as a function of photon energy ($h\nu$) reveals a linear portion around the absorption edge and the optical band gap was determined by extrapolation to zero where the factor $(\alpha h\nu)^{1/2} \to 0$. The observed values of E_g^{opt} and B are listed in Table 1.

The values E_g^{opt} were observed to decrease with increased Sb content which may be attributed to structural changes in the host material brought about by alloying effect. The observed trend in E_g^{opt} values is consistent with those calculated for $Sb_{100-X}Sb_X$ by Srivastava et al. [2] using the Shimakawa [16] theoretical formula. They correlated the observed trend to increased average atomization energy due to addition of Sb. E_g^{opt} is a bond-sensitive property which reflects the bond strength [17] and therefore the decreasing E_g^{opt} values may be due to changes in bond angles or bond lengths [18]. According to Mott and Davis [19] model, the degree of disorder and defects present in an amorphous solid dictates the density of localized states near the mobility gap. The presence of higher densities of these localized states is known to shrink E_g^{opt} values in pristine chalcogenide structures [5,20]. In this case it is anticipated that the addition of Sb in the host Se leads to formation of Se-Sb which increases defects and disorder in the films.

In the weak absorption region where $\alpha < 10^4$ cm^{-1}, photon absorption occurs between localized tail states and extended band states. In this region the dependence of α on photon energy is exponential and is in the form of [21]:

$$\ln(\alpha) = \ln(\alpha_0) + (h\nu/E_u), \quad (3)$$

where α_0 is a constant and E_u is the Urbach energy which represents the width of band tails of the localized states in the band gap. Plots of $\ln(\alpha)$ as a function of photon energy (Fig. 4) reveal linear trends from where the values of E_u were determined from the reciprocal of the slope. The values of E_u are shown in Table 1. The values of E_u were observed to increase with Sb content due to increase in density of localized states in the band gap [19,20,22].

The spectral dependence of refractive index (spectral dispersion) was obtained from the envelope method advanced by Swanepoel [23] based on Magnificier et al. [24]. According to this model, in the region of high transmittance ($\alpha \approx 0$), the refractive index is related to the minimum boundary of the envelope function through:

$$n = [N + (N^2 - s^2)^{1/2}]^{1/2}, \tag{4}$$

where

$$N = 2s/T_{\rm m} - (s^2 + 1)/2T_{\rm m}. \tag{5}$$

In the absorption region where $\alpha \neq 0$, then:

$$N = 2s(T_{\rm M} - T_{\rm m})/T_{\rm M}T_{\rm m} + (s^2 + 1)/2, \tag{6}$$

where $T_{\rm m}$ and $T_{\rm M}$ are the envelope functions of transmittance minima and maxima, respectively, and s is the refractive index of the substrate.

The values of s are obtained from substrate transmittance spectrum (T_S), $S = 1/T_s + \sqrt{(1/T_s^2 - 1)}$. The envelopes were constructed using OriginLab version 7 software. The values of n (Fig. 5) were observed to decrease with increasing wavelength but leveled out at higher wavelengths. There was an ascending dependence of n on increasing Sb composition for all wavelengths in which n was measured. This can be justified on the basis of increasing compactness due to addition of heavier Sb atoms (density = 6.68 g/cm^3) as compared to selenium (density = 4.79 g/cm^3). This may also be due to polarizability of the larger Sb atoms (atomic radius = 1.45 Å) as compared to Se (1.16 Å) [25]. The observed values of n were fitted to a function such as the first two terms of the Sellmeier [26] function of the form:

$$n = \sqrt{A_s + B_s\lambda^2/(\lambda^2 - C_s^2)}, \tag{7}$$

where A, B and C are Sellmeier's constants. As an example, the best fitting for $Se_{100-X}Sb_{10}$ was obtained when $n = (3.74 + 4.38\lambda^2/(\lambda^2 - 355^2))^{1/2}$. The fitted function can be used to extrapolate n values beyond the measured wavelength. Such curve fittings are shown in Figure 5 and a summary of the Sellmeier constants is given in Table 2.

In designing devices for spectral dispersion, knowledge of oscillator parameters is paramount. The dispersion of refractive index $n(\lambda)$ was analyzed using the Wemple-Didomenico (WDD) [27] single oscillator model which has the form:

$$n^2 = 1 + \frac{E_{\rm d}E_{\rm o}}{E_{\rm o}^2 - (h\nu)^2}, \tag{8}$$

where $h\nu$ is the incident photon energy and $E_{\rm o}$ and $E_{\rm d}$ are the single oscillator constants representing the effective oscillator energy (also called average energy gap) and dispersion energy respectively. $E_{\rm d}$ is associated with the average strength of interband optical transitions [27]. By plotting $(n^2 - 1)^{-1}$ against $h\nu^2$ (Fig. 6), values of E_o and E_d can be calculated from the slope $(1/(E_{\rm o}E_{\rm d}))$ and the vertical intercept $(E_{\rm o}/E_{\rm d})$. The obtained values of these oscillator constants are listed in Table 1.

The observed value of $E_{\rm o}$ is related to that of $E_{\rm g}^{\rm opt}$ through, $E_{\rm o} \approx 2E_{\rm g}^{\prime\rm opt}$ which agrees with observations by

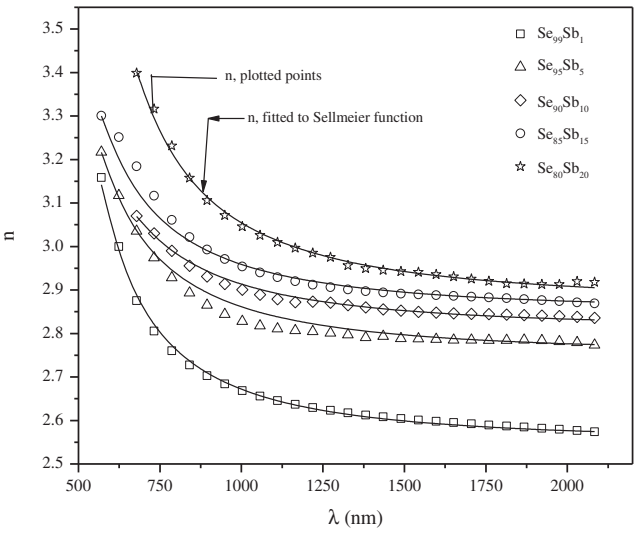

Fig. 5. Spectral dispersion of refractive index (n) for $Se_{100-X}Sb_X$ thin films. Solid curves were determined to fit the Sellmeier dispersion model, regression factor ≈ 0.998.

Tanaka [28]. Farag [29] observed a similar decrease of $E_{\rm o}$ and $E_{\rm g}^{\rm opt}$ with increasing Sb additive in $Se_{100-X}Sb_X$ chalcogenide alloys. Furthermore, an important contribution of the WDD model is the empirical relationship [30] between $E_{\rm d}$ and other physical parameters of the material, $E_{\rm d} = \beta N_c Z_a N_e$, where N_c is the effective coordination number of the cation nearest neighbor to the anion, N_e is the effective number of valence electrons per anion, Z_a is the formal chemical valence of the anion, β is a constant which assumes two values depending on the nature of bonding, $\beta i = 0.26 \pm 0.03$ eV for ionic and $\beta c = 0.37 \pm 0.04$ eV) for covalent bonding [30]. It is observed that the initial variation in the transition strength $E_{\rm d}$ results primarily from changes in the average nearest neighbor coordination number and decrease due to increased ionicities arising from Sb addition.

The static refractive index at zero frequency $n(0)$ is a main indicator of alterations in the structure and it is related to the polarizability of the material through oscillator parameters through [27]:

$$n(0) = [1 + (E_{\rm d}/E_{\rm o})]^{1/2}. \tag{9}$$

Values of $n(0)$ are listed in Table 1 and were observed to increase with Sb content.

The extinction coefficient (k) can be deduced from the relation, $k = \alpha c/2\omega$, where c is the speed of electromagnetic radiation (3×10^8 m/s). The trend of k values (Fig. 7) reveals that the amount of light absorbed or/and scattered decreases with increasing wavelength in the range measured and levels out at longer wavelengths. The band gap can be obtained by plotting $h\nu(2nk)^{1/2}$ against $h\nu$. Such plots consisting of a linear part and an exponential part are shown as an inset in Figure 7. The linear part of the plot obeys the relation [31]:

$$h^2\nu^2(2nk) = (h\nu - E_{\rm g}^{\prime\prime\rm opt})^2. \tag{10}$$

Table 2. Sellmeier constants (A, B and C), N/M^* ratio, mean co-ordination number ($\langle Z\rangle$), average atomization energy (H_s) and average single bond energy ($H_s/\langle Z\rangle$).

Sb (at.%)	Sellmeier constants			$N/M^* \times 10^{55}$ (m^{-3} Kg^{-1})	$\langle Z\rangle$	H_s (KJ/mol)	$H_s/\langle Z\rangle$ (KJ/mol)
	A	B	C				
1	3.35	3.15	409	2.84	2.01	226.76	112.81
5	3.60	3.90	365	2.01	2.05	228.18	111.31
10	3.74	4.38	355	2.23	2.10	229.96	109.50
15	3.33	4.56	340	2.05	2.15	231.74	107.79
20	3.80	4.43	445	1.92	2.20	233.52	106.15

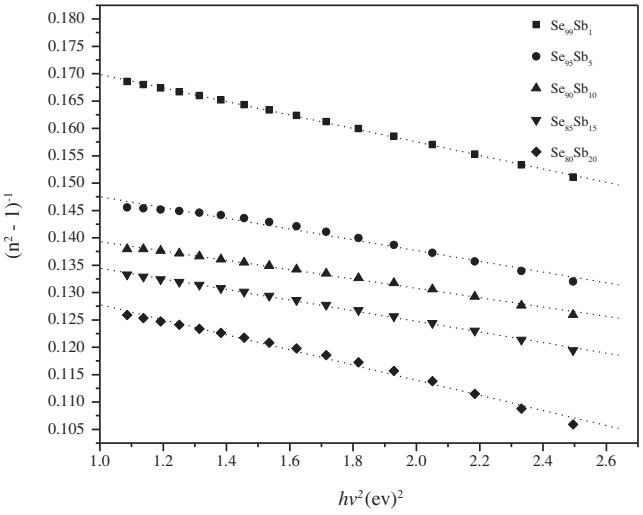

Fig. 6. Plots of refractive index factor (WDD) $(n^2-1)^{-1}$ versus $(h\nu)^2$ for $Se_{100-X}Sb_X$ thin films. Dotted lines are the linear fittings, $R \approx 0.999$.

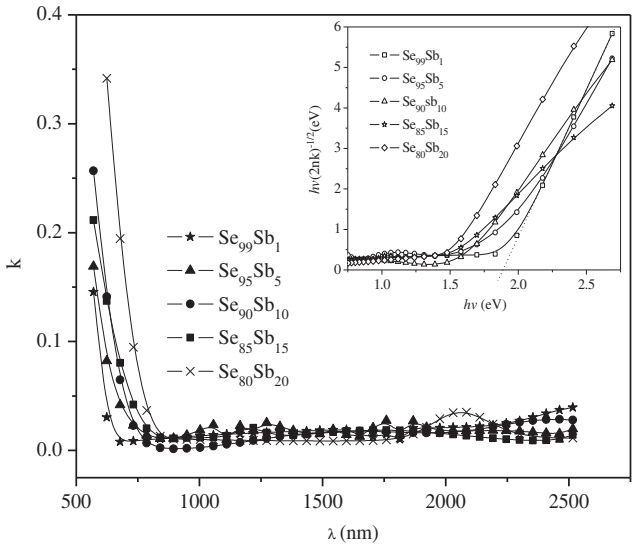

Fig. 7. Extinction coefficient (k) versus wavelength (λ). Inset: Plot of spectral dependence of $h\nu(2nk)^{-1/2}$ on photon energy ($h\nu$) for $Se_{100-X}Sb_X$ thin films. Dotted line is an extrapolation to obtain the $E_g^{\prime\prime opt}$.

From where the values of the optical band gap, $E_g^{\prime\prime opt}$ can be obtained by extrapolation of the linear part where $k \rightarrow 0$, as shown by the dotted line for $Se_{99}Sb_1$.

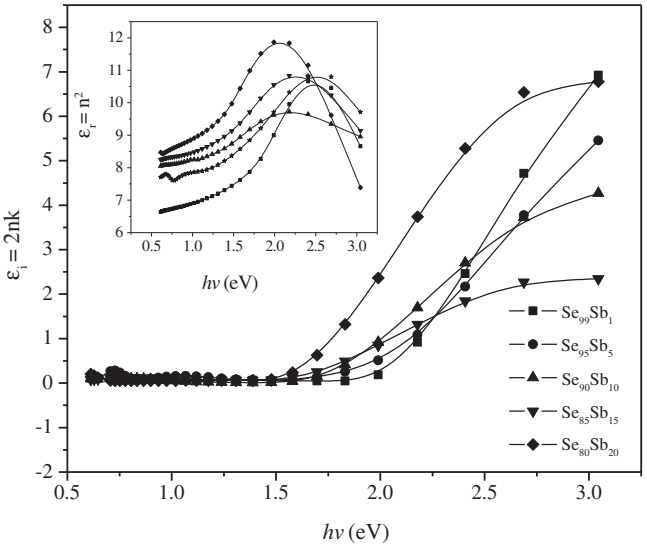

Fig. 8. Spectral dependence of complex dielectric function (ε), real part (ε_r) and imaginary part (ε_i) for $Se_{100-X}Sb_X$ thin films.

The obtained values are presented in Table 1 and are in agreement with E_g^{opt} (Eq. (2)) and $E_g^{\prime opt}$ [28] values obtained by alternative methods.

The complex dielectric constant, ε components (ε_i and ε_r) are related to the optical constants, n and k through $\varepsilon_i = 2nk$ and $\varepsilon_r = (n^2 - k^2)$, where ε_r is the real part and ε_i is the imaginary part of the complex dielectric function. In the region of low absorption where $k \rightarrow 0$, $\varepsilon_r \approx n^2$. The real part controls how radiation is refracted (slowed) while the imaginary part is related to absorption of energy due to dipole dislocation. Figure 8 shows the plots of ε_i and ε_r as a function of photon energy.

The dispersion of refractive index as a function of λ is related to the lattice dielectric constant, ε_L by [32]:

$$n^2 = \varepsilon_L - (q^2/4\pi^2\varepsilon_o c^2)(N/M^*)\lambda^2. \quad (11)$$

For the purpose of definition, N is the carrier concentration, M^* is the effective mass of the carriers, c is the speed of electromagnetic propagation in vacuum, q is the electronic charge and λ is the wavelength of the incident photons. The values of ε_L and N/M^* can be deduced from the vertical intercept ($\lambda = 0$) and slope respectively by plotting n^2 against λ^2 (Fig. 9) [32]. Values of ε_L and N/M^* are entered in Tables 1 and 2, respectively, and the results are consistent with values reported in the literature [18].

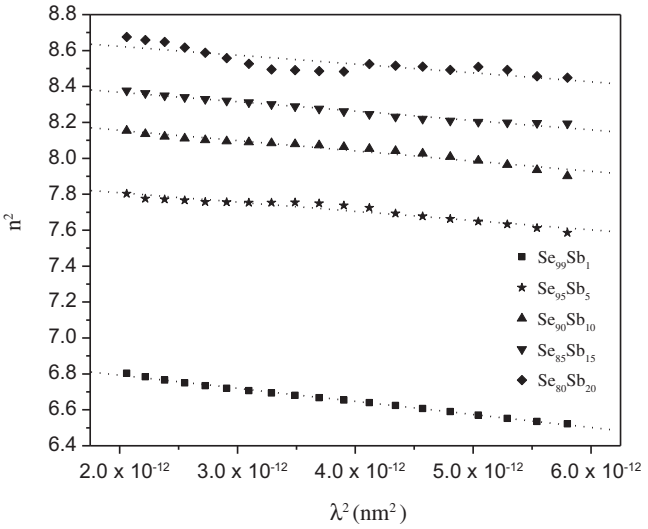

Fig. 9. Plot of n^2 and λ^2 for $Se_{100-X}Sb_X$ thin films. The dotted lines are linear fits with correlation factor ≈ 0.985.

In line with Penn's theory [33]:

$$\varepsilon_{\mathrm{L}} = 1 + (h\omega_{\mathrm{p}}/E_{\mathrm{g}}^{\mathrm{opt}})^2. \tag{12}$$

From where:

$$\omega_p^2 = q^2 N/\varepsilon_{\mathrm{o}}\varepsilon_{\mathrm{L}} M^*, \tag{13}$$

where ω_{p} is the plasma frequency, i.e., the resonant frequency for free electrons about their mean positions. Values of ω_{p} have been calculated and entered in Table 1.

The optical response of a material is related to its optical conductivity (σ) which in turn depends on absorption coefficient (α), refractive index (n) and velocity of photons (c) through $\sigma = \alpha nc/4\pi$ [34]. This parameter σ is frequency (energy) dependent and has dimensions of frequency only valid in the Gaussian system of units. The values of σ at 750 nm for the present system are recorded in Table 1 and the observed trend is similar to those of α and ε_{i}. In the low absorption region the values of σ increase with addition of Sb.

The average coordination numbers $\langle Z\rangle$ of the system were calculated on the basis of topological models proposed by Philips [35] and Thorpe [36]. The obtained values of $\langle Z\rangle$ are recorded in Table 2 and are in the range of 2.01–2.20. For these types of covalent structures, the observation of unusual trends in properties, leading to spiked maxima or minima, is most probable to occur at the rigidity percolation threshold (RPT), $\langle Z\rangle = 2.40$, or at the chemical threshold (CT), $\langle Z\rangle = 2.67$ [37]. The observed physical quantities are in correlation with this hypothesis since gradual changes are recorded for our values of $\langle Z\rangle$ which are <RPT or CT.

The bond energies for heterogeneous compositions, D_{A-B} were calculated from the homonuclear (D_{A-A} and D_{B-B}) bond energies based on Pauling's theory [38]:

$$D_{A-B} = (D_{A-A} \times D_{B-B})^{1/2} + 30(X_A - X_B)^2, \tag{14}$$

where D_{A-A} and D_{B-B} are the bond energies of homopolar bonds for elements A and B respectively and X_{A} and X_B are the corresponding electro negativities respectively. $D_{\mathrm{Se-Se}} = 184.1$ KJ/mol and $D_{\mathrm{Sb-Sb}} = 126.4$ KJ/mol $X_{\mathrm{Se}} = 2.55$ and $X_{\mathrm{Sb}} = 2.05$ [5,39]. The calculated heteropolar bond energy is 161.6 KJ/mol. Results in Table 2 reveal that addition of Sb in the Se host reduces the overall bond energies which reduce the band gap. In order to explain this compositional trend the chemical bond approach (CBA) [20] formed the basis of our argument. According to CBA, in multicomponent covalent structures, the atoms of one species combine more favorably with atoms of different types and these combinations are in order of decreasing bond energies until all valence requirement of each atom is met. Addition of Sb to Se is expected to decrease the average bond energy due to replacement of Se-Se bonds (184.1 KJ/mol) by weaker Se-Sb bonds (183.9 KJ/mol) [5]; however, Mehta et al. [3] have shown that the optimum value of Sb additive in Se-Sb system which the system becomes chemically ordered containing Se-Sb heteropolar bonds is 4 at.% ($\langle Z\rangle = 2.04$). At this composition the system has changed from one to two-dimensional structures (bundles to layers) [3]. Further addition encourages formation of Sb-Sb (126.4 KJ/mol) [3,5] bonds further reducing the cohesive energy of the system. Considering that the Se-Se bond is stronger than Sb-Sb bonds, addition of Sb in the Se host reduces the overall bond energies which reduce $E_{\mathrm{g}}^{\mathrm{opt}}$ and E_{o} values.

According to Pauling [40], for a binary semiconductor of the form $X_\alpha Y_\beta$, the heat of atomization $H_s(X-Y)$ at standard temperature and pressure is the sum of the formation heats (ΔH) and the average heats of atomization (H_s) that correspond to the average nonpolar bond energy of the two atoms X and Y.

$$H_s(X-Y) = \Delta H + 1/2(H_{s,X} + H_{s,Y}). \tag{15}$$

Assuming that α and β are the corresponding atomic combination for X and Y, H_s from equation (15) can be written as [41]:

$$H_s = (\alpha H_{s,X} + \beta H_{s,Y})/(\alpha + \beta), \tag{16}$$

where $H_{S,x}$ and $H_{S,y}$ are the heats of atomization of atoms X and Y respectively. The assumptions referred to are summarized by Mehta et al. [41]. The average single bond energy ($H_s/\langle Z\rangle$) is known to be a direct measure of cohesive energy and hence bond strength. Therefore, it is expected that changes in this parameter with addition of Sb (Tab. 2) will be mirrored in a corresponding change in bond-related properties such as $E_{\mathrm{g}}^{\mathrm{opt}}$ [17]. Earlier studies have emphasized on the correlation between $E_{\mathrm{g}}^{\mathrm{opt}}$ and binding energy. Benoit et al. [42] showed that for certain isolated classes of semiconductors, E_{g} and binding energies are related through, $E_{\mathrm{g}} = a(E_s - b)$, where a and b are constants and E_s is a parameter typical of representing the cohesive energy and a strong indicator of the relative bond strength. In this case average single bond $H_s/\langle Z\rangle$ is a measure of binding energy and can in turn be correlated with the energy gap of isostructural semiconductors [42]. However, this bond approach neglects defects such as dagling bonds and other valence defects. These defects and

contribution of the weaker Van der Waals forces toward bond energies [43] provide weaker links than regular covalent bonds. Increase of Sb results in the decrease of E_g^{opt} and $H_s/\langle Z\rangle$ whereas $\langle Z\rangle$ and H_s increase. The same trend was demonstrated earlier by El-Wahabb et al. and Found et al. [4,5] for Se-Sb chalcogenide alloys deposited by other methods.

4 Conclusion

Amorphous thin films of $Se_{100-X}Sb_X$ (X = 1, 5, 10, 15 and 20) were synthesized by flash evaporation of the premelt quenched bulk samples. The optical properties were correlated to the changing bond parameters resulting from addition of Sb into the Se matrix. The optical absorption mechanism was assigned to indirect transitions across the energy gap with a band gap in the range of 1.5–1.9 eV. The values of E_g^{opt} and E_o decreased with Sb content which is due to decrease in cohesive energy and electronegativity. The values of spectral dependent refractive index were found to ascend with increasing Sb content. The observed trends indicated strong correlation between optical properties and bond parameters both of which show significant dependence on alloy composition.

The authors are grateful for the financial support of African Materials Science and Engineering Network (AMSEN), a Carnegie IAS-RISE network and the University of Botswana through Research Grant R 907. The contribution of Condensed Matter research group, University of Nairobi, where fabrication of samples and spectrophotometric measurements were taken is acknowledged.

References

1. S.M. El-Sayed, G.A.M. Amin, Vacuum **62**, 353 (2001)
2. S. Srivastava, N. Mehta, R.S. Tiwari, R.K. Shukla, A. Kumar, J. Optoelectron. Adv. Mater. **13**, 13 (2011)
3. N. Mehta, M. Zulfequar, A. Kumar, Phys. Status Solidi A **203**, 236 (2005)
4. E.A. EL-Wahabb, S.S. Fouad, M. Fadel, J. Mater. Sci. **38**, 527 (2003)
5. S.S. Fouad, A.H. Ammar, Phys. B: Condens. Matter **229**, 249 (1997)
6. V.I. Mikla, V.V. Mikla, *Metastable States in Amorphous Chalcogenide Semiconductors* (Springer Series in Materials Science 128, Springer-Verlag, Berlin, 2010), p. 101
7. M.J. Kang, T.J. Park, D. Wamwangi, K. Wang, C. Steimer, S.Y. Choi, M. Wuttig, Microsys. Technol. **13**, 153 (2007)
8. V. Pandey, S.K. Tripathi, A. Kumar, Phys. B: Condens. Matter **388**, 200 (2007)
9. A.S. Soltan, J. Appl. Phys. A **80**, 117 (2005)
10. R. Tintu, V.P.N. Nampoori, P. Radhakrishnan, S. Thomas, J. Phys. D: Appl. Phys. **44**, 025101 (2011)
11. A.A. Othman, Thin Solid Films **515**, 1634 (2006)
12. C.M. Muiva, T.S. Sathiaraj, J.M. Mwabora, J. Non-Cryst. Solids **357**, 3726 (2011)
13. G. Lucovsky, Phys. Rev. B **15**, 572 (1970)
14. J. Tauc, in *Amorphous and Liquid Semiconductors*, edited by J. Tauc (Plenum Press, London and New York, 1974)
15. D.L. Wood, J. Tauc, J. Phys. Rev. B **5**, 3144 (1972)
16. K. Shimakawa, J. Non-Cryst. Solids **43**, 229 (1981)
17. N. El-Kabany, Vacuum **85**, 5 (2010)
18. M.A. Majeed Khan, M.W. Khan, J. Alloys Compd. **486**, 876 (2009)
19. N.F. Mott, E.A. Davis, *Electronic Process in Non-Crystalline Materials* (Clarendon Press, Oxford, 1971), p. 210
20. M. Fadel, J. Alloys Compd. **485**, 604 (2009)
21. F. Urbach, Phys. Rev. **92**, 1324 (1953)
22. A.H, Ammar, N.M. Abdel-Moniem, A.A.M. Farag, M. El-Sayed, Phys. B: Condens. Matter **407**, 356 (2012)
23. R. Swanepoel, J. Phys. E: Sci. Instr. **17**, 896 (1984)
24. J.C. Magnificier, J. Gasiot, J.P. Fillard, J. Phys. E: Sci. Instr. **9**, 1002 (1976)
25. I. Sharma, S.K. Tripathi, P.B. Barman, Appl. Surf. Sci. **255**, 2791 (2008)
26. G. Ghosh, M. Endo, T.I. Wasalu, J. Lightwave Technol. **12**, 1338 (1994)
27. S.H. Wemple, M. Di-Domenico, J. Phys. Rev. B **3**, 1338 (1971)
28. K. Tanaka, Thin Solid Films **66**, 271 (1980)
29. El-Sayed M. Farag, J. Opt. Materials **29**, 397 (2009)
30. S.H. Wemple, Phys. Rev. B **7**, 3767 (1973)
31. J. Tauc, R. Grigorovici, A. Vancu, Phys. Status Solidi B **15**, 627 (1966)
32. M.M. Wakkad, E.K. Shokr, S.H. Mohamed, J. Non-Cryst. Solids **265**, 157 (2000)
33. N.M. Ravindra, S. Auluck, V.K. Shrivastava, Phys. Status Solidi B **93**, K155 (1979)
34. J. Pankove, *Optical Processes in Semiconductors* (Dover, New York, 1975), p. 91
35. J.C. Phillips, J. Non-Cryst. Solids **34**, 153 (1979)
36. M.F. Thorpe, J. Non-Cryst. Solids **57**, 355 (1983)
37. P. Kumar, R. Thangaraj, T.S. Sathiaraj, Phys. Status Solidi A **206**, 1465 (2009)
38. L. Paulings, *The Chemical Bonds* (Cornell University, New York, 1976), p. 92
39. A.H. Moharan, Appl. Phys. A **66**, 515 (1998)
40. L. Pauling, J. Phys. Chem. **58**, 662 (1954)
41. N. Mehta, S.K. Agrahari, A. Kumar, Mater. Lett. **61**, 837 (2007)
42. C. Benoit, P. Aigrain, M. Balkanski, *Selected Constants Relative to Semiconductors* (Pergamon Press, New York, 1961), p. 36
43. A.A. Othman, K.A. Aly, A.M. Abousehly, Thin Solid Films **515**, 3507 (2007)